

Supporting information

Enriched Pseudocapacitive Lithium Storage in Electrochemically Activated Carbonaceous Vanadium(IV, V) Oxide Hydrate

*Joseph F. S. Fernando,^{*ab} Dumindu P. Siriwardena,^{ab} Konstantin L. Firestein,^{ab} Chao Zhang,^{ab} Joel E. von
Treifeldt,^{ab} Courtney-Elyce M. Lewis,^{ab} Tony Wang,^{ac} Deepak P. Dubal,^{ab} and Dmitri V. Golberg^{*abd}*

*^aCentre for Materials Science, Queensland University of Technology (QUT), Brisbane,
Queensland, 4000, Australia.*

*^bSchool of Chemistry and Physics, Queensland University of Technology (QUT), Brisbane,
Queensland, 4000, Australia.*

*^cCentral Analytical Research Facility (CARF), Institute for Future Environments (IFE),
Queensland University of Technology (QUT), Brisbane, Queensland, 4000, Australia.*

*^dInternational Center for Materials Nanoarchitectonics (MANA), National Institute for Materials
Science (NIMS), Namiki 1-1, Tsukuba, Ibaraki 3050044, Japan.*

Corresponding Authors

*E-mail: jf.fernando@qut.edu.au

*E-mail: dmitry.golberg@qut.edu.au

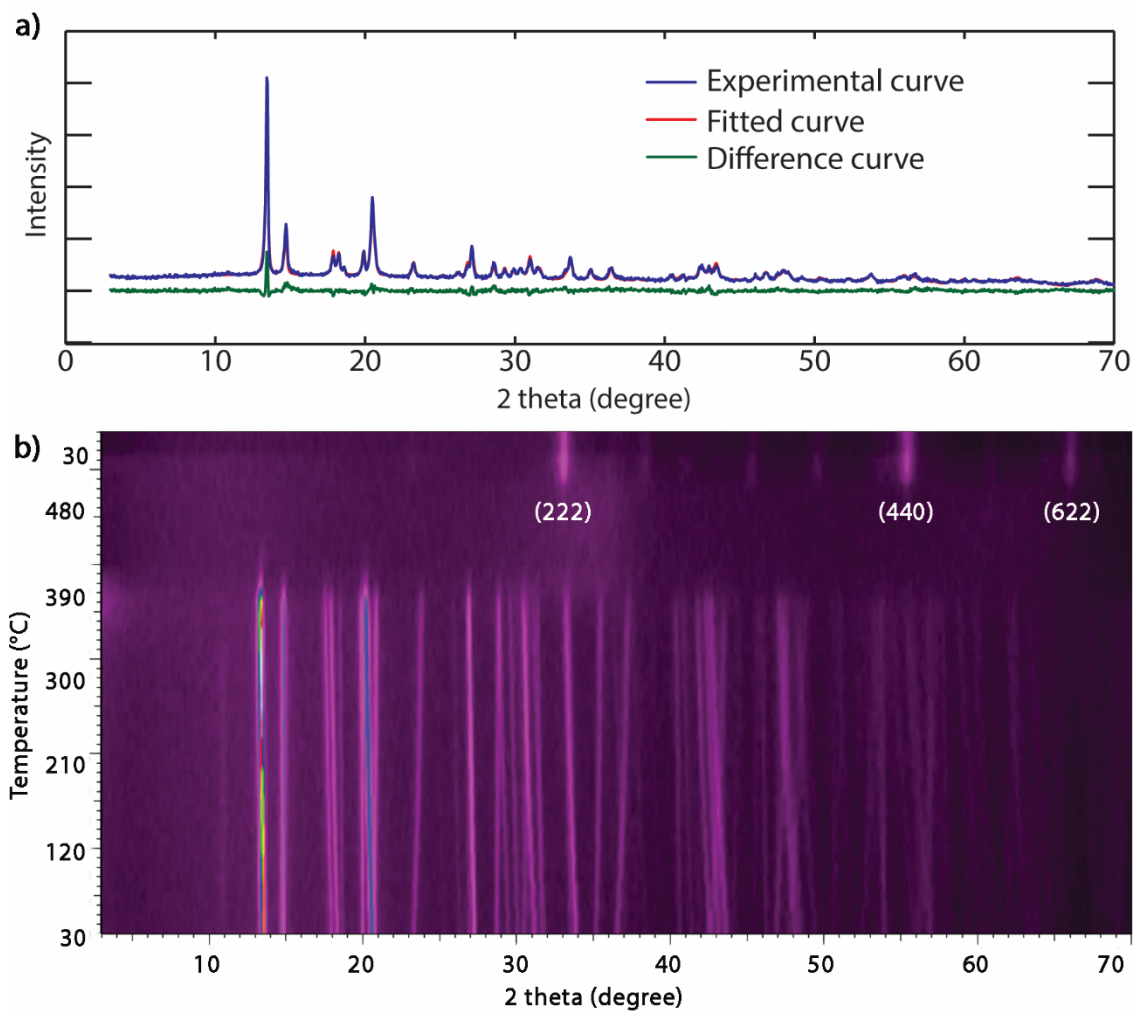


Figure S1. a) Rietveld refinement of vanadyl glycolate structure from PDF: 00-049-2497. b) *In-situ* XRD monitoring of thermal decomposition of vanadyl glycolate complex to C-V₂O₃ composite: The lowest temperature required to form the intermediate C-V₂O₃ was determined using an *in situ* XRD heating experiment. We observed a decrease in lattice parameter for *a* and *c* axes, and lattice parameter increase for *b* axis of vanadyl glycolate. The change in *b* axis is dominating, which induces unit cell volume expansion as temperature ramps up. After 390 °C, there is a sudden collapse of crystalline structure to an amorphous form. At 500 °C, the cubic crystal structure of V₂O₃ was formed. The final structure consists of both cubic and trace amounts of rhombohedral phases of V₂O₃.

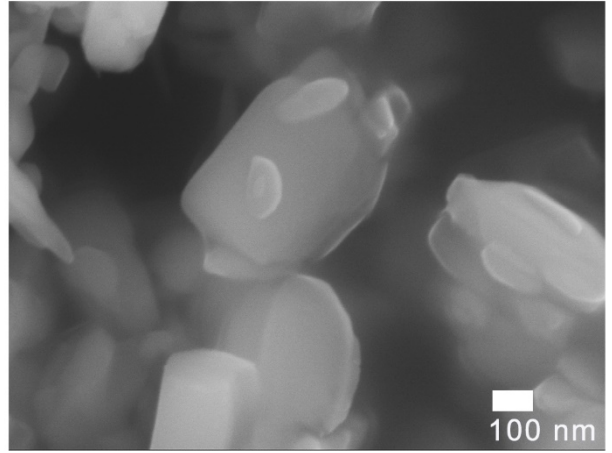
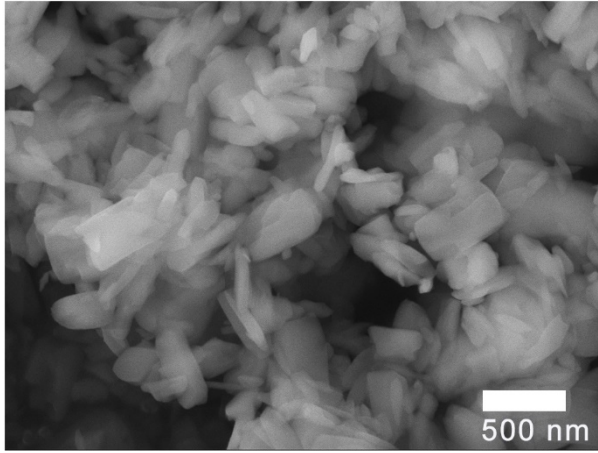


Figure S2. SEM images of VGC product.

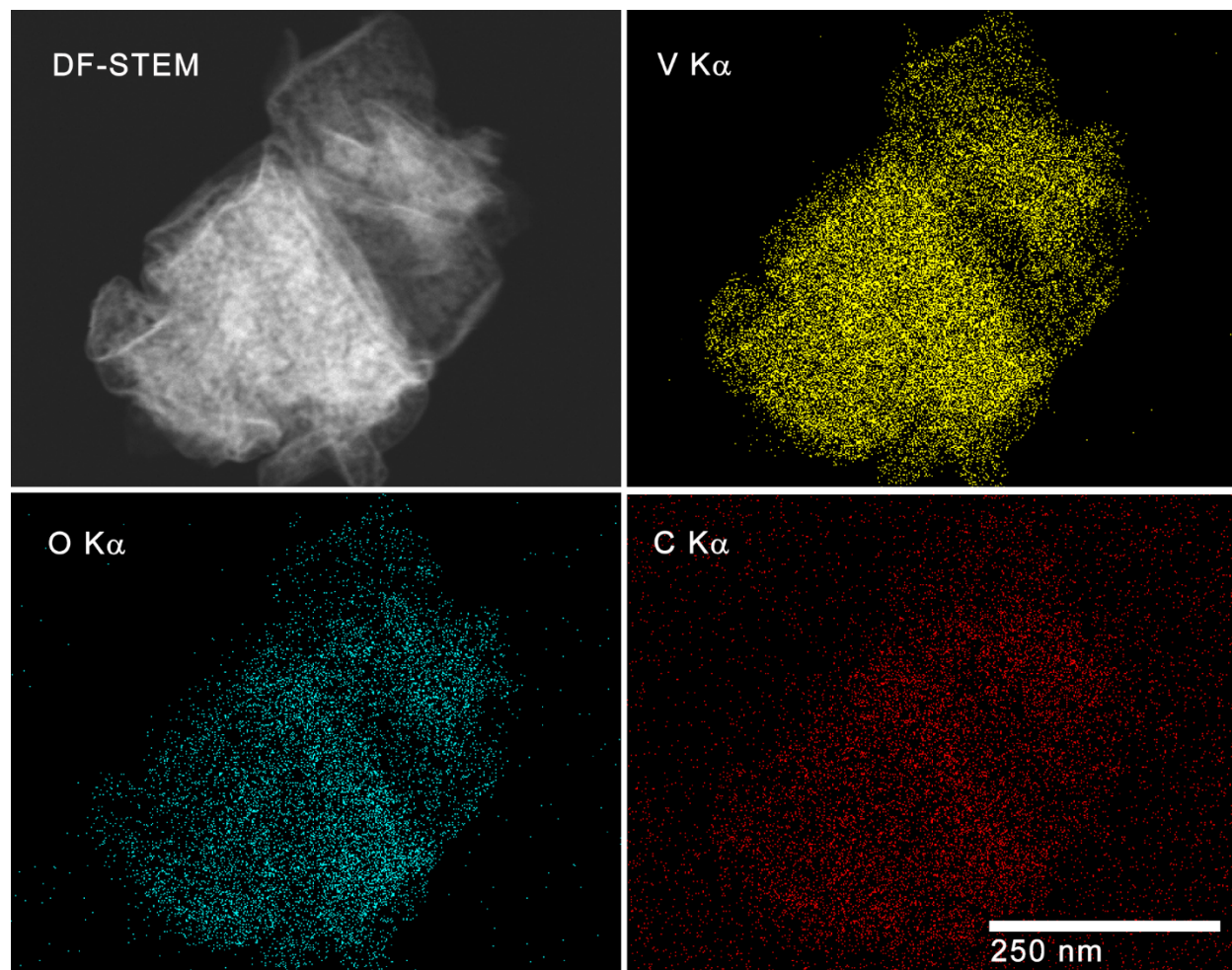


Figure S3. DF-STEM image and the corresponding spatially-resolved EDX maps for individual elements in the V₂O₃ – carbon composite.

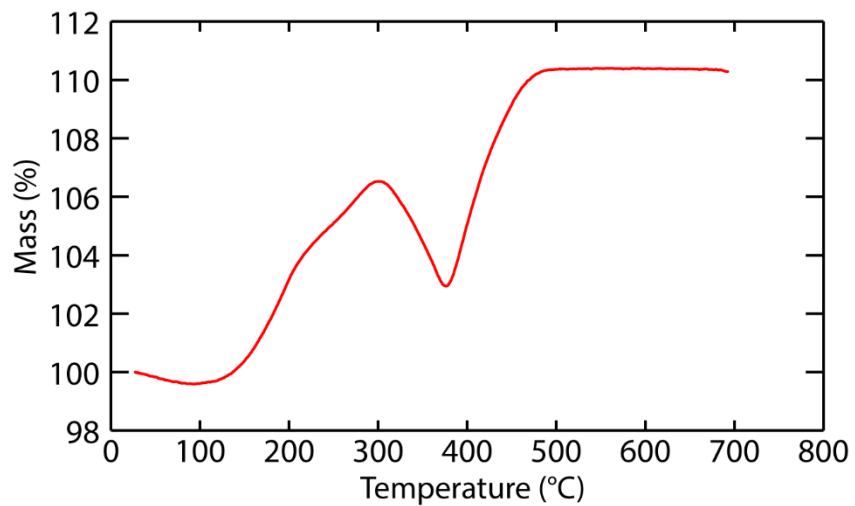


Figure S4. TGA curve for C-V₂O₃. TGA was carried out in air from 25 °C to 700 °C at a heating rate of 5 °C/min. Oxidation of V₂O₃ to V₂O₅ leads to a mass gain, and mass loss at about 325 °C is attributed to the decomposition of carbon.

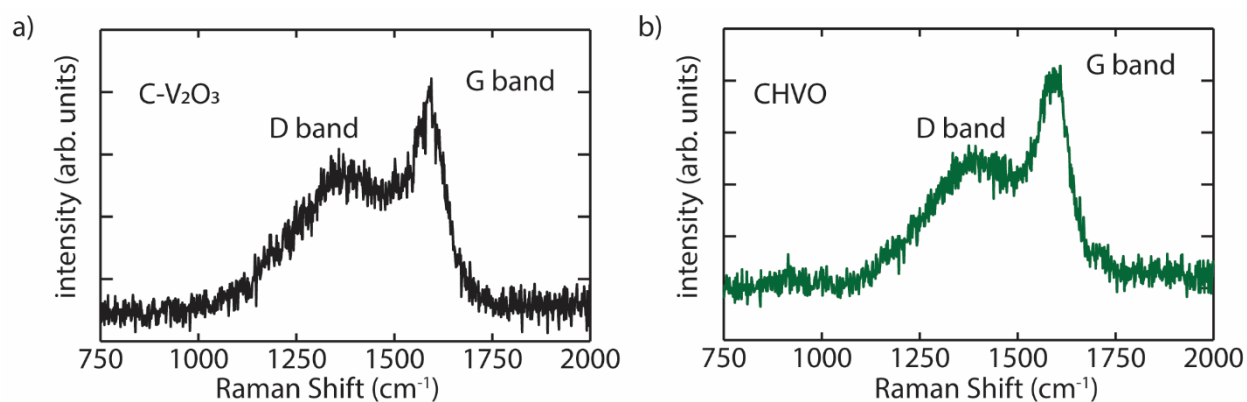


Figure S5. Raman spectra acquired from a) C-V₂O₃ and b) CHVO samples showing D and G bands of amorphous carbon.

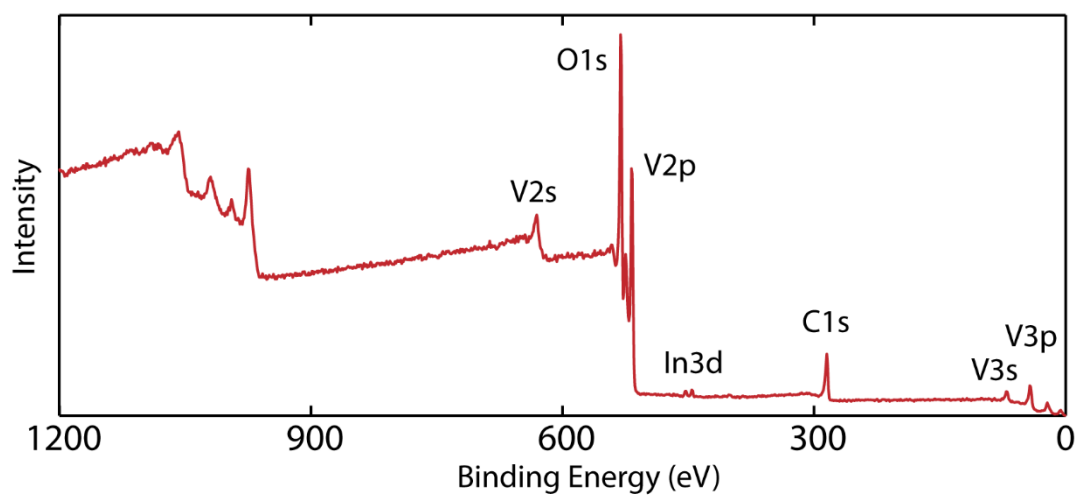


Figure S6. XPS survey spectrum of CHVO showing the existence of V, O and C in the material. Faint In3d signal is from the indium substrate used for sample preparation.

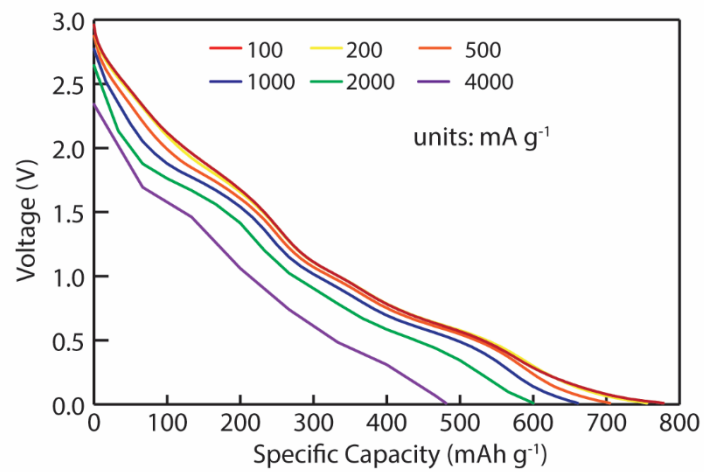


Figure S7. Discharge curves for CHVO material at different specific currents. Curves correspond to the 10th discharge of each current step in the rate capability test.

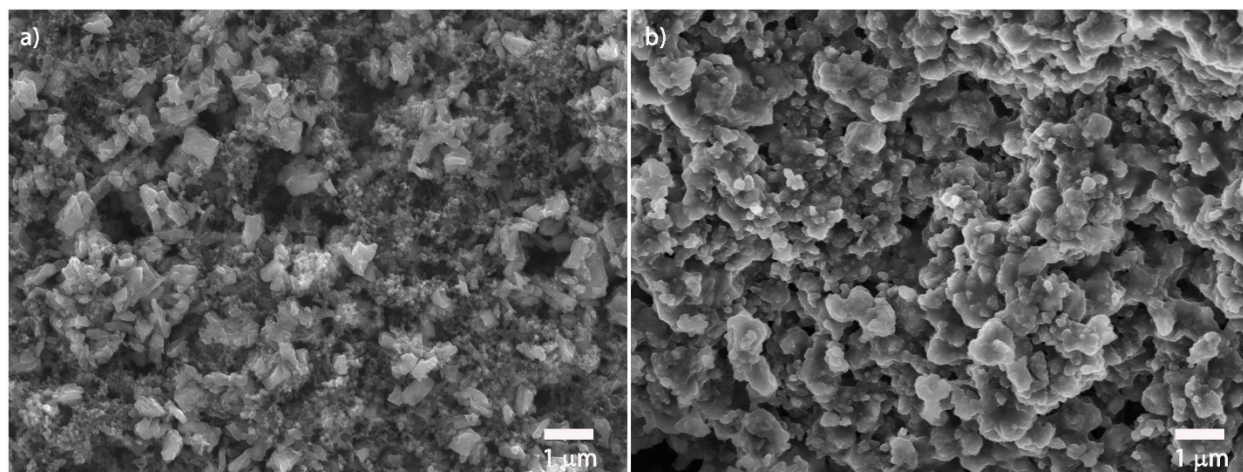


Figure S8. a) SEM image of a CHVO electrode slurry coated on the Cu current collector. b) SEM image of the electrode after operating the battery for 600 cycles at a specific current of 1000 mA/g.

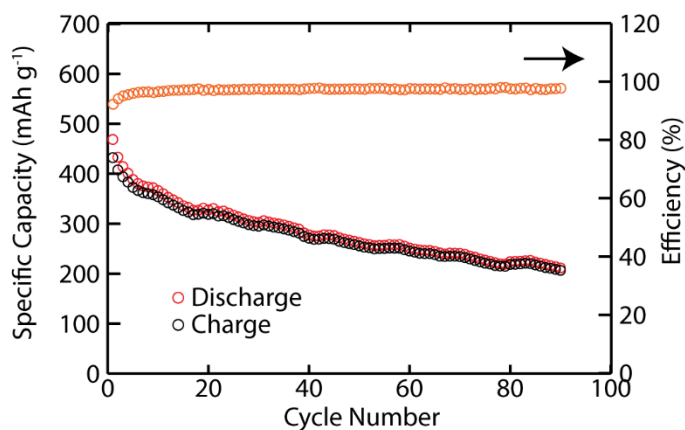


Figure S9. Cycling performance of fully hydrated vanadium oxide ($V_5O_{12}.6H_2O$) at a specific current of 1000 mA g^{-1} . The fully hydrated form of CHVO ($V_5O_{12}.6H_2O$) can be obtained *via* exposure to moisture or direct mixing with water. This material delivered a very low specific capacity of 211.6 mAh g^{-1} after 90 cycles, as opposed to 664.4 mAh g^{-1} by $V_5O_{12}.0.4H_2O$ material. Hence, too much hydration clearly has a detrimental effect to the battery performance. Another study specifically investigated the effect of water content on the electrochemical performance (as cathode at high potentials) of a hydrated vanadium pentoxide ($V_2O_5.nH_2O$) xerogel.¹ Those authors found that significant amounts of water can lead to adverse reactions with lithium, leading to low specific capacity. In their study $V_2O_5.0.3H_2O$ xerogel displayed the best specific capacity (185 mAh g^{-1} – as cathode). The fully hydrated form has been recently investigated for an aqueous Zn-ion battery.²

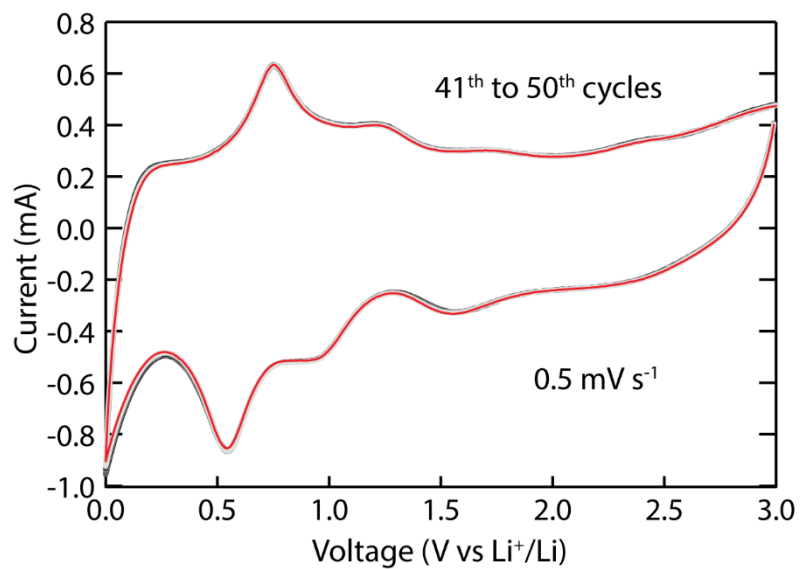


Figure S10. 41st to 50th CV profiles of CHVO electrode (scan rate: 0.5 mV s⁻¹) after galvanostatic (dis)charge of a cell for 40 cycles at a specific current of 100 mA g⁻¹.

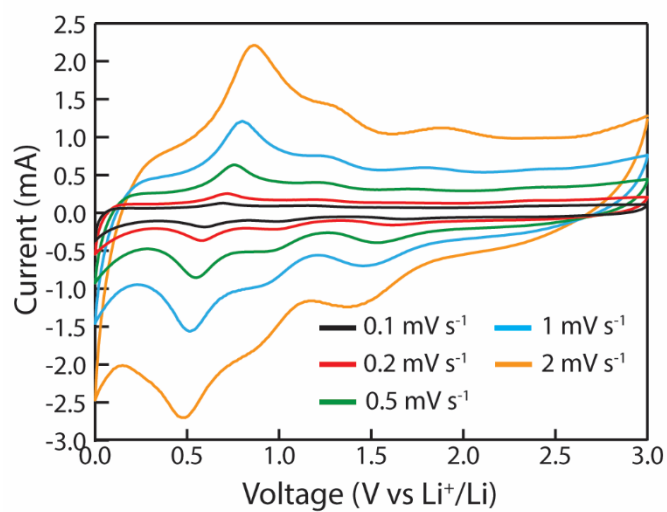


Figure S11. CV profiles for CHVO material collected at different scan rates from 0.1 to 2 mV s^{-1} . CV curves at different scan rates were collected after cycling the half cell for 30 cycles at a specific current of 100 mA g^{-1} .

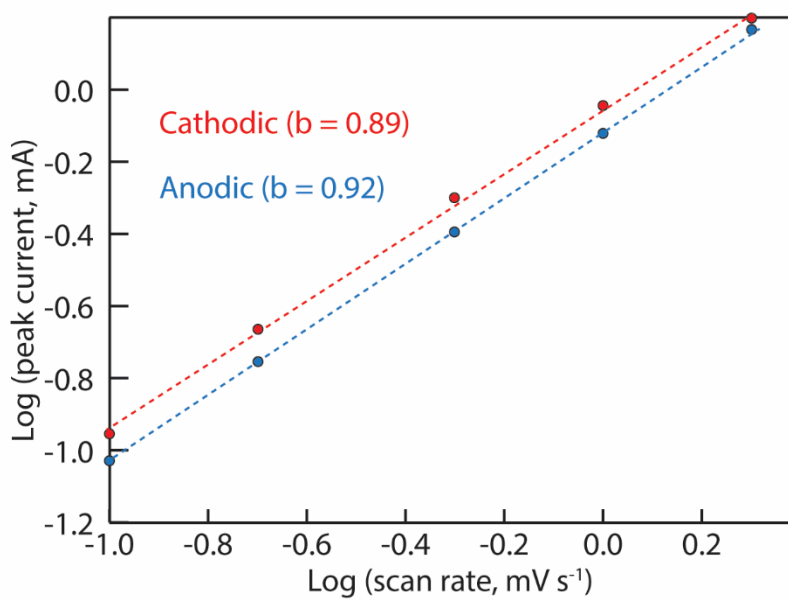


Figure S12. log (peak current) vs log (scan rate) plots for anodic and cathodic peaks at 1.20 V and 0.96 V, respectively.

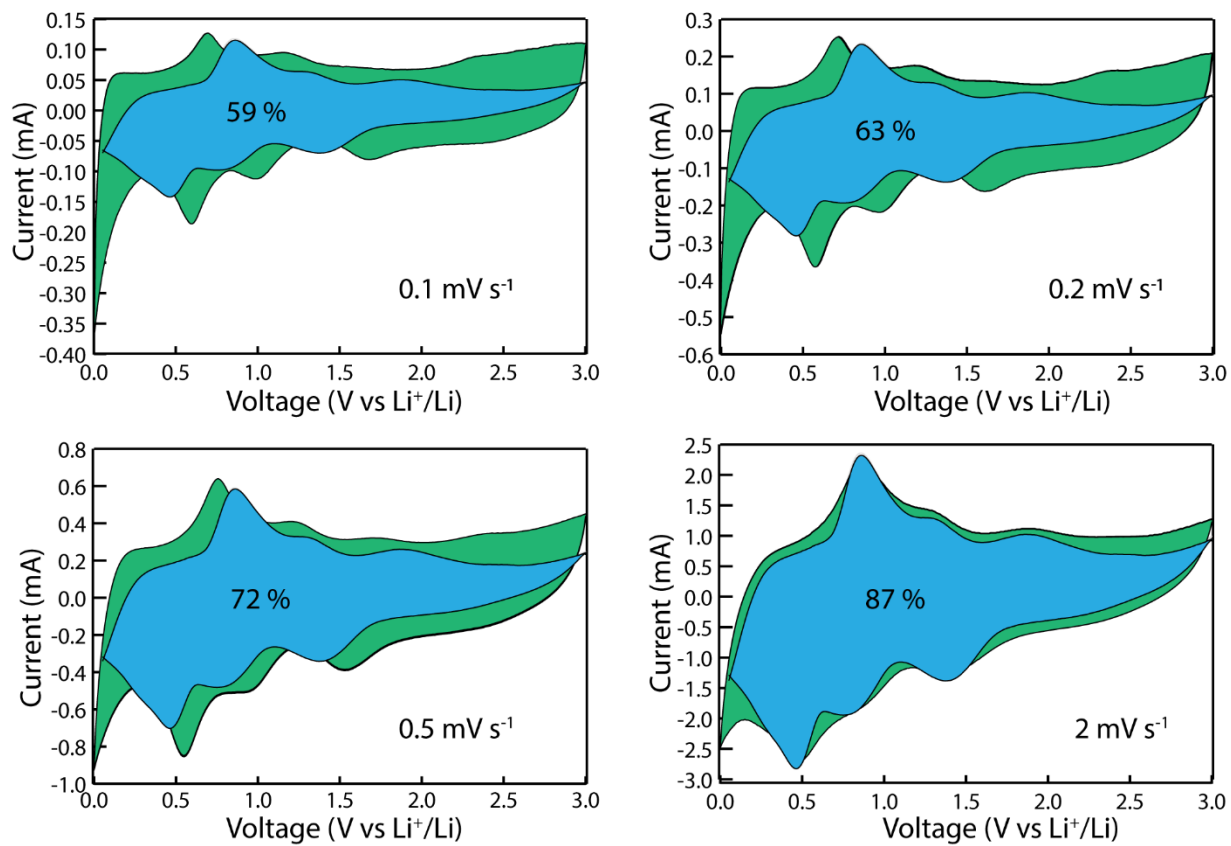


Figure S13. Capacitive (light blue) contribution at scan rates of 0.1, 0.2, 0.5 and 2 mV s⁻¹.

Calculation of Q_t and Q_s

For a known voltage scan rate, the total gravimetric charge (Q_t) was found from the CV curve according to the following:

$$Q_t = \frac{1}{2} \times \frac{\text{integrated absolute area under CV curve}}{\text{scan rate} \times \text{active material mass}}$$

Q_t was determined for all scan rates (0.1, 0.2, 0.5, 1 and 2 mV s^{-1}). The intercept of plot of Q_t vs $v^{-1/2}$ gives the surface controlled capacitive charge (Q_s) (Figure S12).³

$$Q_t = kv^{-1/2} + Q_s$$

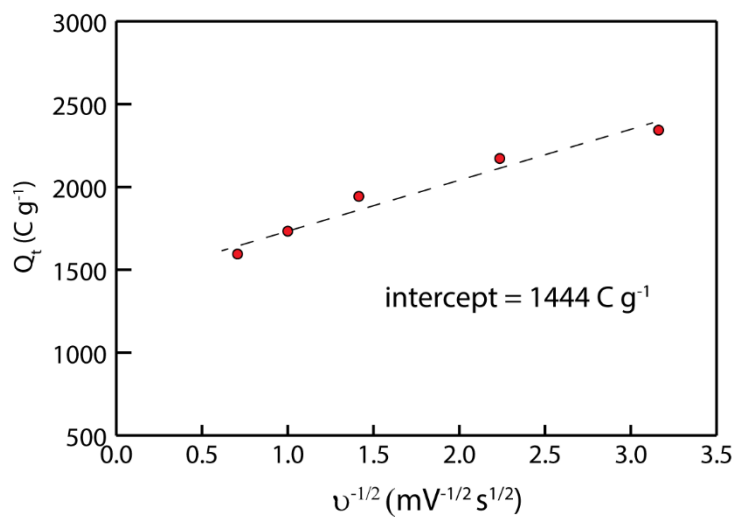


Figure S14. Plot of total gravimetric charge (Q_t) vs reciprocal square root of scan rate ($v^{-1/2}$)

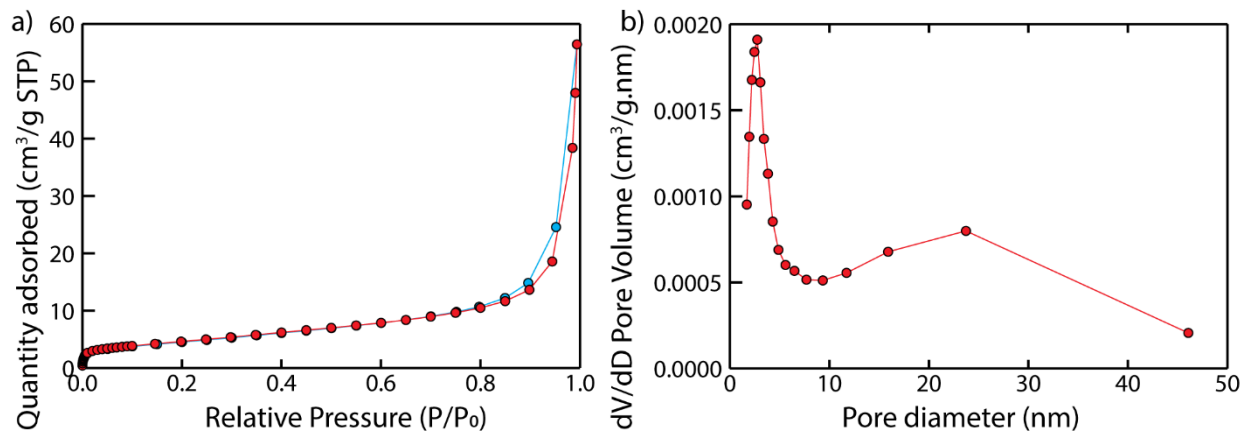


Figure S15. a) N₂ adsorption-desorption isotherm recorded for CHVO material at 77 K. b) Pore size distribution as determined from the adsorption isotherm by BJH method.

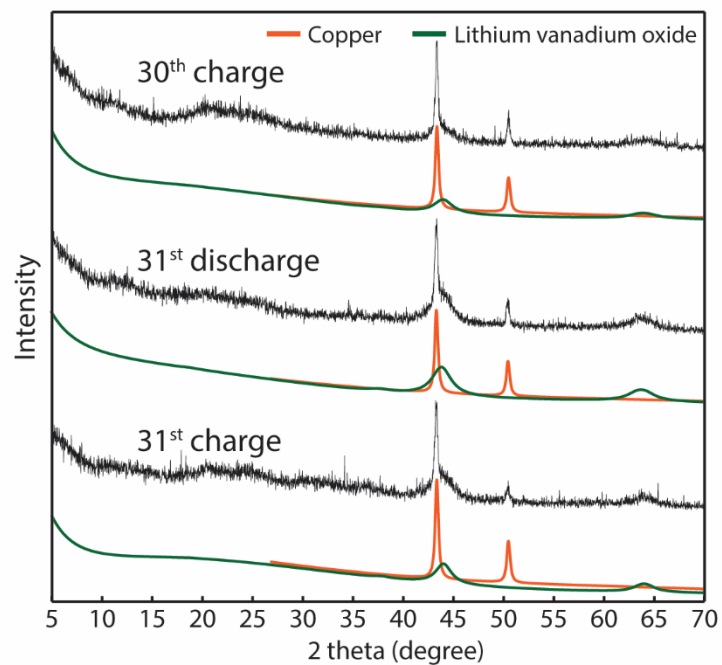


Figure S16. *Ex situ* XRD data of CHVO electrodes separated from disassembled batteries at 30th charge, 31st discharge and 31st charge.

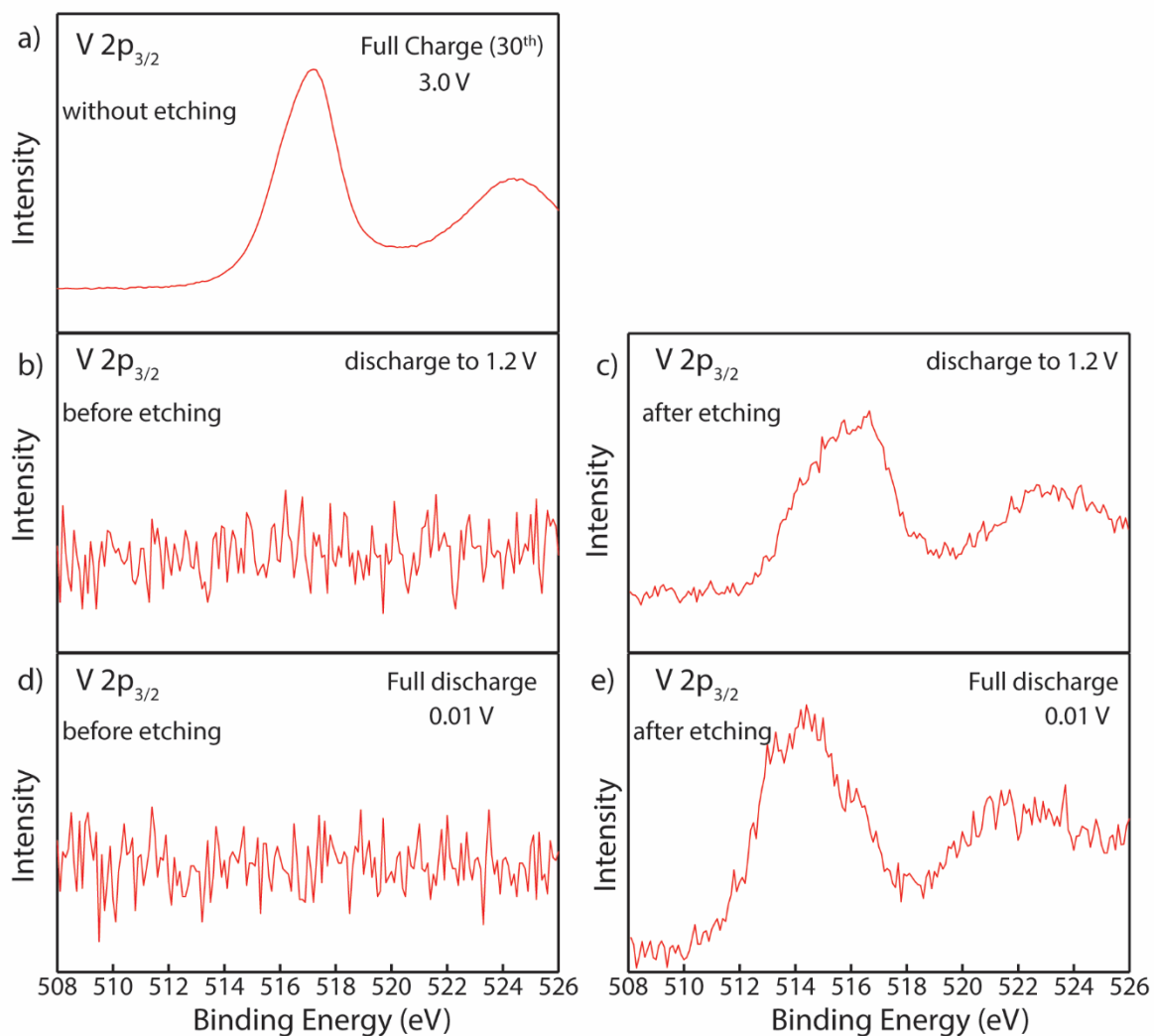


Figure S17. a) V 2p *ex-situ* XPS data for fully charged (3.0 V) electrode without any etching. b) and c) V 2p *ex-situ* XPS data for partially discharged (1.2 V) electrode before and after etching. d) and e) V 2p *ex-situ* XPS data for fully discharged (0.01 V) electrode before and after etching. Etching was performed using the argon gas cluster ion source (10 keV, Ar1000⁺) in Kratos Axis supra XPS machine for 1 min.

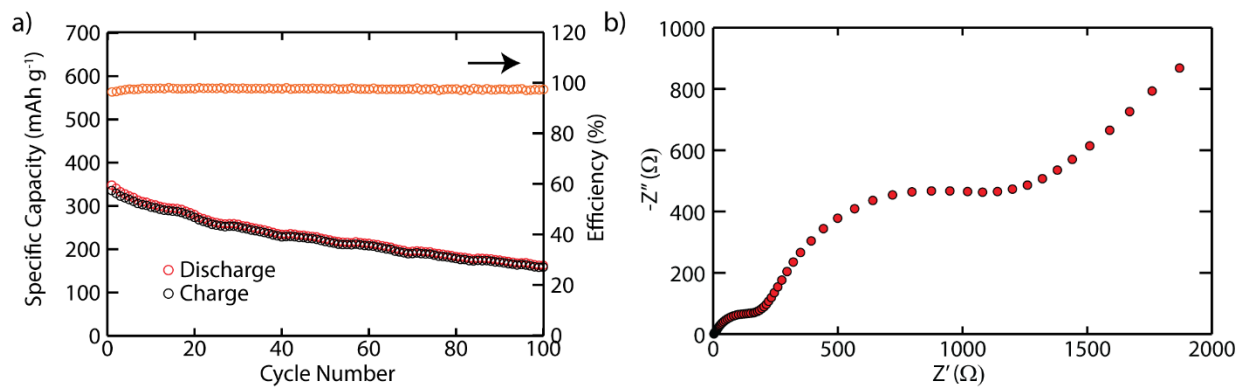
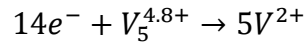


Figure S18. a) Cycling performance of HVO (*i.e.* after removing the carbon component; the battery was cycled at a specific current of 1000 mA g^{-1}). b) EIS curve of HVO/Li cell recorded after the 20th dis(charge) cycle.

Estimation of theoretical specific capacity of CHVO

Assuming an overall conversion of V_5O_{12} to VO:



Molar mass (M_w) of $V_5O_{12} \cdot 0.4H_2O = 453.90 \text{ g mol}^{-1}$

$$\text{theoretical capacity} = \frac{n \times F}{3.6 \times M_w} = 827 \text{ mAh g}^{-1}$$

F is the Faraday constant.

Considering the relative amounts of $V_5O_{12} \cdot 0.4H_2O$ and amorphous carbon in the composite:

$$827 (V_5O_{12} \cdot 0.4H_2O) \times 0.95 + 470 (\text{amorphous carbon}) \times 0.045 = 807 \text{ mAh g}^{-1}$$

Table S1: The electrochemical performance of vanadium oxide-based electrodes cycled to potentials below 1 V (in literature) compared to the CHVO materials produced in this work.

Material	Reversible Capacity (mAh g⁻¹)	Current Density (mA g⁻¹)	Cycle number
Vanadium oxide aerogel ⁵	1000 700	118 590	50
2D V ₂ O ₅ sheet network ⁶	600	100	40
V ₂ O ₅ nanobelt array ⁷	650	1200	50
mixed-valance VO _x microspheres ⁸	1050	100	140
Amorphous V ₂ O ₅ ⁹	600	100	50
Amorphous vanadium oxide/graphene ¹⁰	900	200	100
2D vanadium oxide @carbon nanosheet ¹¹	793 802	500 1000	60 200
Sandwich like V ₂ O ₅ /graphene ¹²	1006 734	500 900	300 60
This work (CHVO)	1161 675 525 381	100 1000 1000 4000	150 200 600 250

References

1. Y. Wang, H. Shang, T. Chou and G. Cao, *J. Phys. Chem. B*, 2005, **109**, 11361-11366.
2. N. Zhang, M. Jia, Y. Dong, Y. Wang, J. Xu, Y. Liu, L. Jiao and F. Cheng, *Adv. Funct. Mater.*, 2019, **29**, 1807331.
3. Z. Chen, V. Augustyn, X. Jia, Q. Xiao, B. Dunn and Y. Lu, *ACS Nano*, 2012, **6**, 4319-4327.
4. S. J. Yang, S. Nam, T. Kim, J. H. Im, H. Jung, J. H. Kang, S. Wi, B. Park and C. R. Park, *J. Am. Chem. Soc.*, 2013, **135**, 7394-7397.
5. V. Augustyn and B. Dunn, *Electrochim. Acta*, 2013, **88**, 530-535.
6. Y. Xu, M. Dunwell, L. Fei, E. Fu, Q. Lin, B. Patterson, B. Yuan, S. Deng, P. Andersen, H. Luo and G. Zou, *ACS Appl. Mater. Interfaces*, 2014, **6**, 20408-20413.
7. Y. Wang, H. J. Zhang, W. X. Lim, J. Y. Lin and C. C. Wong, *J. Mater. Chem.*, 2011, **21**, 2362-2368.
8. D. Zhao, L. Zheng, Y. Xiao, X. Wang and M. Cao, *ChemSusChem*, 2015, **8**, 2212-2222.
9. O. B. Chae, J. Kim, I. Park, H. Jeong, J. H. Ku, J. H. Ryu, K. Kang and S. M. Oh, *Chem. Mater.*, 2014, **26**, 5874-5881.
10. X. Sun, C. Zhou, M. Xie, T. Hu, H. Sun, G. Xin, G. Wang, S. M. George and J. Lian, *Chem. Commun.*, 2014, **50**, 10703-10706.
11. X. Wang, W. Jia, L. Wang, Y. Huang, Y. Guo, Y. Sun, D. Jia, W. Pang, Z. Guo and X. Tang, *J. Mater. Chem. A*, 2016, **4**, 13907-13915.
12. X. Wang, Y. Huang, D. Jia, W. K. Pang, Z. Guo, Y. Du, X. Tang and Y. Cao, *Inorg. Chem.*, 2015, **54**, 11799-11806.